Fowler-Nordheim tunneling in thin SiO_2 films

1992 Smart Mater. Struct. 1 197

(http://iopscience.iop.org/0964-1726/1/3/002)

Smart Mater. Struct. 1 (1992) 197–201. Printed in the UK

Fowler–Nordheim tunneling in thin SiO_2 films

N M Ravindra and Jin Zhao

Department of Physics, New Jersey Institute of Technology, Newark, NJ 07102, USA

Received 13 April 1992, accepted for publication 29 June 1992

Abstract. An analysis of the Fowler–Nordheim tunneling (FNT) theory and its application to temperature-dependent current–voltage characteristics of very thin films SiO_2 on silicon, is presented. The final results are believed to provide the most complete examination of FN emission theory and predict the breakdown electric field in thin SiO_2 films. The role of the roughness, at the Si–SiO_2 interface, in determining the FNT current in these structures is also discussed.

1. Introduction

Oxidized silicon surfaces are used on virtually all of today's integrated circuits and silicon devices. It is very important to understand the electrical properties of SiO_2 for making high quality devices. From past studies, it is well known that the FNT contributes to current conduction in SiO_2 films [1–3]. FNT is the fundamental current conduction mechanism in micromachined cold cathode arrays [4]. These arrays, constructed from conducting protrusions such as cones and wedges that are surrounded by an extraction electrode [5–8], have potential applications in microsensors, high-speed electronics and displays. Unlike thermionic emission where refractory metals have to be heated to high temperatures, micromachined cold cathode arrays can operate at any temperature. One of the applications of silicon as a smart material is in the form of such arrays. The advantage of using silicon as a smart material lies in its highly improved technology that is fully compatible with conventional very large scale integration (VLSI) integrated circuit (IC) processes. The other advantage is the ability to focus a beam of electrons of a given energy into the smallest possible spot and with the highest possible current. In the present work, an investigation of the current–voltage characteristics, in the temperature range of 100–350 K, of thermally grown SiO_2 films on silicon, is presented.

At room temperature, our experimental data is in accordance with the FNT equation [2]

$$J = CF^2 e^{-\beta/F} \tag{1}$$

$$C = \frac{q^3 m_0}{16\pi^2 \hbar m_{ox} \phi_b} \qquad \beta = \frac{4(2m_{ox})^{1/2}}{3q\hbar}\phi_b^{3/2} \tag{2}$$

where, F is the uniform electric field, q is the electronic charge, m_0, m_{ox}, are the electron mass in free space and in the oxide, respectively, h is Planck's constant, and ϕ_b is the barrier height. The FN plot parameters based on static current–voltage characteristics in this study are comparable to the other independent experimental results available in the literature. This is presented in table 1.

However, at temperatures other than 300 K, our data cannot fit the simplified FNT equation (1). This is because the barrier height and effective mass generally decrease with increasing temperature [9–12]. This has motivated us to re-examine the factors which were ignored in earlier studies [2].

Using the earlier reported results of high-resolution transmission electron microscopy (HRTEM) [13, 14], a discussion of breakdowns caused by interface protrusions is presented.

2. Theory

The high field imposed across the oxide, which is necessary for tunneling (approximately in the range of 7.5–10 MV cm^{-1}), results in a large density of electrons

Table 1. Tunneling results from present and past work at 300 K. Negative electrodes are n-type Si ⟨100⟩.

Parameters	Present work	Ravindra[3]	Weinberg [16]	Krieger [9]	Osburn [10]
Slope (MV cm^{-1})	270	260	238.5	237	246
ϕ_b' (eV)	3.05	3.05	2.9	2.89	2.96
m_{ox}/m_0	0.46	0.45	0.5	0.36	0.5

0964-1726/92/030197+05$07.50

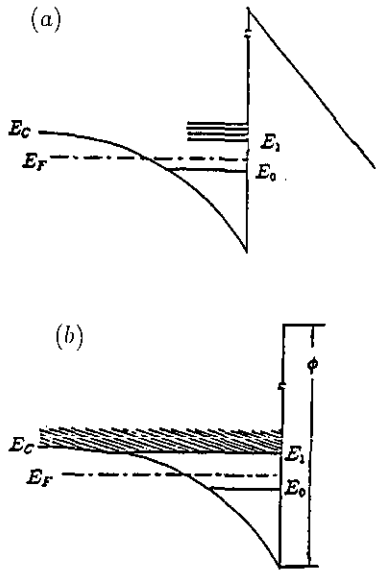

Figure 1. (a) The strong band bending in silicon leads to the formation of a narrow potential well with quantized energy levels or subbands ($E_0, E_1 \ldots$). (b) The energy levels are separated into two sources of emission. A continuum beginning with E_1 and a single subband beginning at E_0.

which are confined to a narrow potential well at the interface. This leads to quantization of the energy to the interface [15], see figure 1(*a*). E_0 remains discrete while the higher energy levels are merged into a continuum beginning with E_1. The continuum is assumed to obey bulk statistics and tunneling from it will be small compared to tunneling from E_0. This is illustrated in figure 1(*b*). All the electrons within the same subband have the same energy associated with motion perpendicular to the interface. They will also have the same tunneling probability. The transmission probability current per electron (Q), for level n, is found by the following equation [16]

$$Q = \frac{4\pi}{Z_n^{3/2}}\left(1+\frac{m_{ox}E_n}{m_{Si}\phi_b'}\right)^{-1}\left(\frac{m_{ox}E_n}{m_{Si}\phi_b'}\right)^{1/2}\frac{E_n}{\hbar} \times e^{-\beta(E_n)/F_{ox}} \tag{3}$$

$$\beta(E_n) = \frac{4\sqrt{2m_{ox}}(\phi_b' - E_n)^{3/2}}{3q\hbar}$$

$$E_n = \frac{Z_n}{2^{1/3}}\left(\frac{q\hbar}{m_{Si}^{1/2}}F_{Si}\right)^{2/3} \tag{4}$$

where, E_n represents the energies of the quantized levels measured from the bottom of the conduction band, and Z_n are zeros of the Airy function, $Z_0 = 2.338$. To complete the solution of the tunneling current, Q has to be multiplied by carriers in the lowest subband. It is given by ΘN, where $N = \epsilon_{ox}F_{ox}/q$ (Gauss law). N is the number of electrons per unit area at the interface and Θ is its fraction residing in the lowest subband, and ϵ_{ox}, ϵ_{Si} are the dielectric constants of the oxide and silicon, respectively

$$J(E_0) = q\theta N Q(E_0) = CF_{ox}^2 e^{-\beta(E_0)/F_{ox}} \tag{5}$$

where

$$C = \theta\left(1+\frac{m_{ox}E_0}{m_{Si}\phi_b'}\right)^{-1}\left(\frac{2q^2m_{ox}}{m_{Si}^2\phi_b'}\right)^{1/2}\frac{\epsilon_{ox}^2}{\epsilon_{Si}}2\pi \tag{6}$$

$$\beta(E_0) = \frac{4(2m_{ox})^{1/2}}{3q\hbar}\left(\phi_b'\right)^{3/2} \qquad \phi_b' = \phi_b - E_0. \tag{7}$$

From earlier studies [11], it is known that just as the energy gap decreases with increasing temperature, the barrier height also decreases. Approximately, $d\phi_b/dT \sim dE_g/dT$

$$\phi_{bt} = \phi_b' + \beta\Delta T \tag{8}$$

where

$$\beta = \left(\frac{\phi_{b0}}{E_g}\right)\left(\frac{dE_g}{dT}\right) \qquad \frac{dE_g}{dT_{Si}} = -2.3\times10^{-4}\ \text{eV K}^{-1}. \tag{9}$$

3. Experimental details

The oxides were grown at 800 °C on single-crystal silicon wafers (n-type, Czochralski) of ⟨100⟩ orientation and 2 ohm cm resistivity. Prior to oxidation, the silicon wafers were cleaned using conventional cleaning procedures including the RCA technique followed by a HF dip and thorough rinsing with deionized water. MOS capacitors, intended for breakdown measurements, were fabricated by evaporating 700 nm thick Al electrodes on the oxide (front) through a metal mask to form Al dots of 0.08 cm (32 mil) in diameter. Al was evaporated for a back contact after removing the oxide on the back of the wafers. A post-metallization anneal was done in forming gas (10% H_2 in N_2) at 450 °C for 30 min.

Oxide thickness measurements were carried out, using a Gaertner automatic ellipsometer, at nine points on the wafer. The mean deviation in the thickness was found to be ~2%. For determination of the oxide thickness, a refractive index of 1.465 (at 632.8 nm corresponding to the He–Ne laser) for SiO_2 was used. Breakdown voltage measurements were made using a Rucker and Kolls automatic prober stepper model 682. Steady state I–V measurements were made on these capacitors in order to determine the FNT current. Cross section samples for HRTEM were prepared using a combination of mechanical and ion-beam polishing methods. High-resolution phase contrast images of the interface were taken at a Scherzer defocus value of 65 nm and ⟨110⟩ orientation using a JEOL 200CX TEM at 200 kV with a 0.27 nm point to point resolution [13].

4. Results and discussion

Static current–voltage measurements were made in the temperature range 100–350 K. The results of these measurements are fitted to the FNT equation (5). In figure 2, the FNT plots at temperatures of 100, 200 and

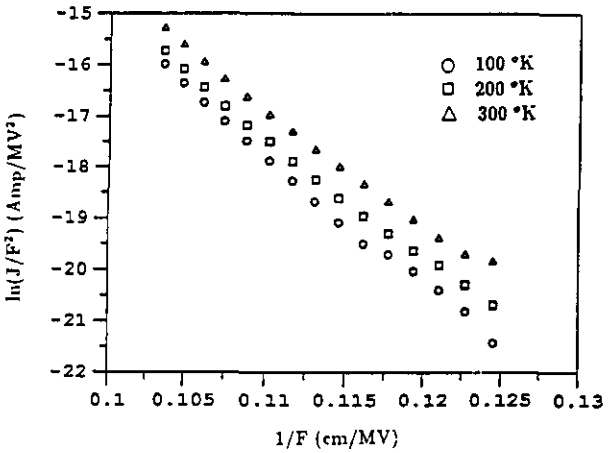

Figure 2. The FN plots of tunneling data from silicon into SiO_2 at temperatures of 100, 200 and 300 K.

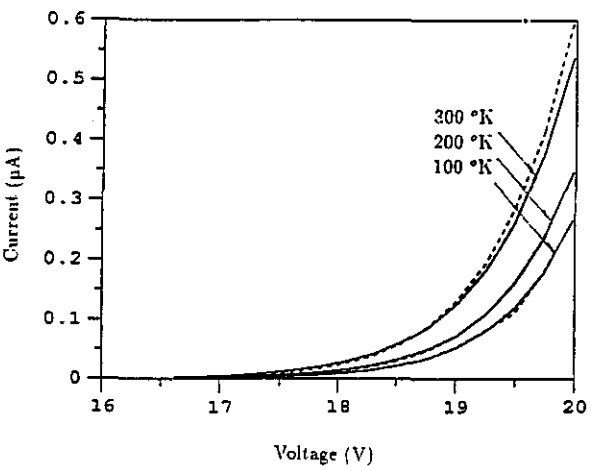

Figure 3. The comparison of the experimental data (solid curve) with the calculated data (dotted curve) of the *I–V* characteristic at temperature of 100, 200 and 300 K.

300 K are presented. As can be seen in the figures (within experimental errors) the plot of $\ln(J/F^2)$ versus $1/F$ is indeed linear. This not only demonstrates temperature-dependent FN slopes, but also implies that the FNT current is temperature dependent. Although tunneling, in itself, is temperature dependent, the number of electrons incident on the barrier is dependent on temperature.

Considering equations (6) and (7), the parameters Θ, ϕ_b', E_0, m_{ox}, m_{Si}, and ϵ_{ox}, ϵ_{Si} are temperature dependent. However, E_0 is very small compared to ϕ_b, and ϵ_{ox}, ϵ_{Si}, m_{Si} affect only the pre-exponent C. Therefore, we assume that the influence of temperature on E_0, ϵ_{ox}, ϵ_{Si} and m_{Si} to be negligible. The barrier height ϕ_b, from the silicon conduction band edge to the oxide conduction band, has been determined to be 3.25 eV [17]. The temperature dependent ϕ_{bt} can be derived using equation (8). The slopes of the FN plot, ϕ_{bt}, and equation (7) lead to the evaluation of the effective mass m_{ox} given in table 2.

Using the slope obtained from the FNT plot in figure 2(*a*), the barrier height and effective mass from table 2, and equation (5), the current–voltage characteristics are calculated and presented in figure 3. It can be seen that the calculations are in good agreement with experimental data at different temperatures. In figure 3, results of the comparison of experimental and calculated I–V characteristics are presented for temperatures of 100, 200 and 300 K.

As an illustration of the influence of non-uniformity in oxide thickness on FNT current, we have considered a $\sim$ 20 nm thick SiO_2 film. Assuming a 10% non-uniformity (decreasing) in the oxide thickness, and 20 V supply across the oxide, using equation (5), the current ratio I_{18nm}/I_{20nm} is calculated. These results are presented in table 2 for different temperatures. As can be seen in the table, a decrease in T_{ox} by 10% has led to an increase in the FNT current by ~20%. Furthermore, taking 1 mA current as the breakdown criteria [18] in equation (5), the temperature-dependent breakdown fields are predicted in table 2. So far, we have only considered the ideal case of a flat Si–SiO_2 interface. In fact, no surface is entirely free of height irregularities. As shown in figure 4, the protrusions at the Si–SiO_2 interface are of the order of $\sim$ 2 nm in $\sim$ 20 nm thick SiO_2 films.

Such protrusions enhance the field and produce locally intense tunneling currents. To simplify the problem, we assume a homogeneous distribution of electric field in SiO_2 films. Such a distribution is shown in figure 5.

$$I = 2\pi \int_0^a rJ\,\mathrm{d}r = 2\pi C \int_0^a rF_{ox}^2(r) \times \mathrm{e}^{-\beta(E_0)/F_{ox}(r)}\,\mathrm{d}r \tag{10}$$

where

$$F_{ox}(r) = \frac{V}{d-z} = \frac{V}{d-b+rb/a}$$

$$z = -r\frac{b}{a} + b. \tag{11}$$

Comparing I with I_0, a current gain caused by the protrusion can be derived as follows

$$G = \frac{I}{I_0} = \frac{2\int_0^a rF_{ox}^2(r)\mathrm{e}^{-\beta(E_0)/F_{ox}(r)}\,\mathrm{d}r}{a^2F_{ox}^2\mathrm{e}^{-\beta(E_0)/F_{ox}}} \tag{12}$$

Table 2. Temperature-dependent slope ϕ_{bt}, m_{ox}/m_0, current ratio, and F_{max}.

Temperature (K)	100	150	200	250	300	350
Slope (MV cm^{-1})	281	280.5	277	274	270	266
ϕ_{bt} (eV)	3.17	3.141	3.111	3.081	3.050	3.018
m_{ox}/m_0	0.50	0.499	0.486	0.476	0.462	0.448
F_{max} (MV cm^{-1})	13.1	13.09	12.99	12.91	12.97	12.67
I_{18nm}/I_{20nm}	20.51	20.40	19.7	19.12	18.37	17.65

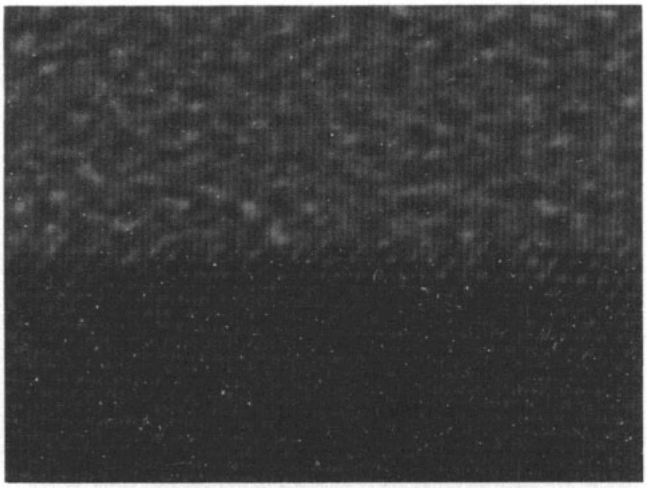

Figure 4. High-resolution transmission electron micrograph of the Si–SiO_2 interface for an oxide thickness of 22 nm. The point to point distance is 0.314 nm [13].

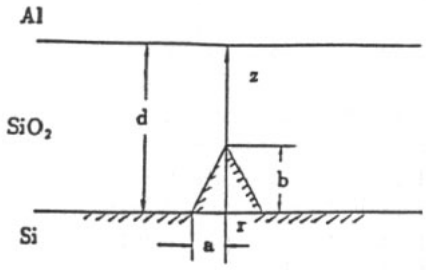

Figure 5. A silicon tip at the Si–SiO_2 interface

where, I and I_0 are the currents with and without the protrusions, respectively. From TEM micrographs used in figure 4, for d = 20 nm, b = 2 nm, and a = 1 nm, and using equation (12), we obtain G = 3.45. Thus, a 3.45 times enhancement in current gain is expected to result in a local breakdown.

Furthermore, after tunneling out of the cathode irregularity, electrons drift through the oxide under the influence of the average applied field. There is an energy transfer from the field to the electrons at the rate of FJ W cm^{-3} where F and J are the field and current density, respectively. To simplify further, we assume that the initial heat production is confined to a cylindrical filament in the oxide with spreading regions in metal and silicon. The heat flow equation in cylindrical coordinates with no angular dependence is [19]

$$CD\frac{\partial T}{\partial t} = FJ + K\left[\frac{1}{r^2}\frac{\partial}{\partial r}\left(\frac{r^2\partial T}{\partial r}\right) + \frac{\partial^2 T}{\partial z^2}\right] \quad (13)$$

where C is the specific heat, D the density, T the temperature, and K the thermal conductivity. In the case of very thin filaments, radial flow will dominate. The steady-state solution of equation (6) (neglecting the temperature variation across the filament) is

$$T = (FJ/2K)a^2 \ln(d/r) \qquad T = 0 \text{ at } r = d \quad (14)$$

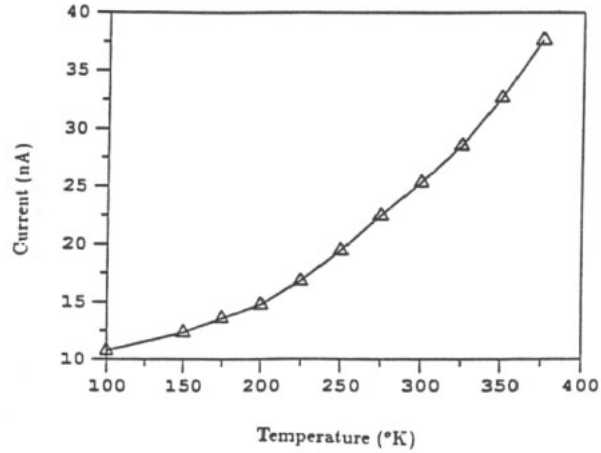

Figure 6. Current versus temperature for emission from silicon at E = 9.3 MV cm^{-1}.

where the ambient temperature at the cylindrical surface $r = d$ is taken to be zero. Therefore, T is the temperature rise. To obtain a realistic estimate of T, we replace d with w, the oxide width. In this limit,

$$T = (FJ/2K)a^2 \ln(w/a). \quad (15)$$

For example, taking $\ln(w/a)$ = 2.3, K = 10^{-2} W cm^{-1} K^{-1}, E = 10^7 V cm^{-1}, and a = 2 nm, a temperature rise of 50 °C occurs with J = 10^6 A cm^{-2}. This leads to a 1.5 times enhancement in current gain. Figure 6 shows the FNT current increase with increasing temperature for certain values of applied electric field.

An increasing FNT current density promotes a temperature rise leading to a stable local high-temperature region. This is expected to result in enhanced probability of local breakdown.

5. Conclusions

A detailed investigation of the application of FNT, to interpret the temperature-dependent static current–voltage characteristics of thin SiO_2 films in silicon, has been presented in the above study. Modification to the FNT equation has been sought in order to correct for the temperature-dependent effective mass and barrier height. Calculations of the current–voltage characteristics have been shown to be in accord with experimental data. The influence of the presence of protrusions at the Si–SiO_2 interface as well as Joule heating on the current and breakdown fields has been discussed. The above studies are expected to lead to a better understanding of FNT in MOS and vacuum microelectronic devices and structures.

Acknowledgments

The authors are thankful to the New Jersey Commission of Science and Technology and SEMATECH for partial financial support.

References

[1] See, for example
Sze S M 1981 *Physics of Semiconductor Devices* 2nd ed (New York: Wiley) p 497

[2] Lenzinger M and Snow E H 1969 *J. Appl. Phys.* **40** 278

[3] Ravindra N M, Russo O L, Fathy D, Narayan J, Heyd A R and Vedam K 1988 *Mater. Res. Soc. Symp. Proc. (Pittsburg)* **105** p 169

[4] Orvis W J, McConaghy C F, Ciarlo D R, Yee J H and Hee E W 1989 *IEEE Trans. Electron Devices* **ED-36** 2651

[5] Busta H H, Zimmerman B J, Tringides M C and Spindt C A 1991 *IEEE Trans. Electron Devices* **ED-38** 2558

[6] Spindt C A, Holland C E and Stowell R D 1984 *J. Physique* C **9** 45

[7] Howell D F, Groves R D, Lee R A, Patel C and Williams H A 1989 *Vacuum Microelectronics '89 (Inst. Phys. Conf. Ser. No 99)* (Bristol: Institute of Physics) p 81

[8] Brodie I and Muray J J 1988 *The Physics of Microfabrication* (New York: Plenum)

[9] Krieger G and Swanson R M 1981 *J. Appl. Phys.* **52** 5710

[10] Osburn C M and Weitzman E J 1972 *J. Electrochem. Soc.* **119** 603

[11] Ravindra N M, Kumar K S and Srivastava V K 1982 *Phys. Status Solidi* **70** 623

[12] Sharma A C, Ravindra N M, Auluck S and Srivastava V K 1983 *Phys. Status Solidi* **120** 715

[13] Ravindra N M, Narayan J, Fathy D, Srivastava J K and Irene E A 1987 *J. Mater. Res.* **2** 216

[14] Carim A H and Sinclair R 1987 *Mater. Lett.* **5** 94

[15] Weinberg Z A 1977 *Solid State Electron.* **20** 11

[16] Weinberg Z A 1982 *J. Appl. Phys.* **52** 5052

[17] Williams R 1969 *J. Appl. Phys.* **40** 278

[18] Osburn C M 1986 *MCNC Memorandum* March

[19] Ridley B K 1975 *J. Appl. Phys.* **46** 998